Trident Wind Collaborative
Collaborate Innovate Generate

APRIL
2022

Technical Design Report Milestone

Prepared for the 2022 Collegiate Wind Competition Organizers and the U.S. Department of Energy

COLLEGIATE
WIND COMPETITION
U.S. DEPARTMENT OF ENERGY

JAMES MADISON
UNIVERSITY

Faculty Advisors

Dr. Stephen Keith Holland
Dr. Jonathan Miles
Mr. Edwin Clamp

Joshua Bautch
Secondary Lead of Electronic Design

Alexandra Davis
Primary Lead of Controls and Electronic Design

Garrett Downs
Primary Lead of Generator and Electronic Design

Ban Mansoor
Secondary Lead of Electronic Design

Nicole Peterson
Secondary Lead of Electronic Design

Matthew Porchetta
Secondary Lead of Generator and Structure & Foundation Design

Colby Schneider
Primary Lead of Structure & Foundation Design

Brian Sweet
Primary Lead of Rotor Design

Table of Contents

Executive Summary

With the focus of the CWC 2022 competition being on offshore development, the Trident Wind Collaborative (TWC), from James Madison University (JMU), identified three primary objectives of enhancing prototype control using a wind speed sensing device, reducing thrust at high wind speeds through implementing a blade pitch mechanism, and designing a mounting structure to address the sand bed anchoring requirements. An existing prototype from the 2021 JMU team served as a reference design to modify for alignment with the CWC 2022 Rules and Regulations (R&R). The identified objectives served to enhance the capabilities of prior JMU prototype designs for the revised competition requirements.

The team began with the planning and information gathering phase of the design process by learning wind concepts, understanding requirements, benchmarking prior competition designs, and identifying challenges encountered by prior JMU competition teams. While several alternatives were considered, the team identified a three-blade, active pitch, horizontal axis rotor as the design most suited to meet competition objectives. The blade concept that was ultimately selected for competition was a Wortmann FX60-126 root airfoil with a SG6042 tip profile designed for a tip-speed ratio of 3.0. The blades were 3D printed with Onyx filament, a strong and flexible carbon fiber reinforced nylon material. An active pitching mechanism consisting of lever arms, ball joints, and a push plate attached to a Actuonix PQ12 linear servo, was designed to adjust the angle of attack at wind speeds greater than 11m/s to maintain constant power output and reduce rotor thrust. The pitching system will be a broad power regulator and will be fine tuned by the digitally controlled current sink.

Electrical power is produced from a team-designed direct drive, three-phase axial flux permanent magnet generator composed of two magnetic rotors, each with 12 neodymium magnets and 9-coil stator. The hand wound stator coils, each with 200 turns of 26-gage magnet wire, were designed to match required generator torque with simulated blade rotor torque and rotational speed characteristics to maximize power production. The three phase AC generated power is rectified, regulated to a constant voltage and distributed throughout the system to an actuator, sensors, microcontroller, the PCC, and load using commercially available connectors and wires. A digitally controlled current sink into a load resistor serves as the turbine system's maximum power point tracking load.

For turbine safety tasks a second Actuonix PQ12 linear servo was incorporated into the nacelle to pull a cabled disc brake. When the turbine is in a state of emergency, such as when power is lost or the emergency stop button is pressed, the brake system brings the turbine rotors to a complete stop. Similar to the 2021 JMU team, TWC has incorporated three current-voltage sensors, a wide-input 12 V output buck-boost converter, and 120 VAC - 12 VDC power supply for restart conditions. New this year is the incorporation of a Rev. C wind speed sensor to better identify state conditions and stop relying on an optical encoder and power output for state recognition.

The prototype is controlled by two Arduino Pro Minis, one in the load-side NEMA enclosure and the other in the turbine NEMA enclosure. The two microcontrollers communicate via optically isolated serial communications through HCPL 2200 ICs. The turbine controller monitors generator power, buck-boost converter power, rotor rotational speed, and emergency stop conditions. The load controller serves as the primary controller, incorporating information from the turbine to implement control algorithms that monitor the state conditions of the turbine and adjust load and pitch settings.

This report details the TWC team's design decisions, control scheme, testing results, and commissioning checklist to be implemented at the competition. Due to planning and design for manufacturing, a fully functional turbine was fabricated and demonstrated at JMU, as seen in Figure 1. Testing results indicated that the balanced design objectives were achieved.

Figure 1: Fully assembled turbine prototype.

1.0 Design Objectives

Three primary objectives for the TWC prototype were to enhance controls using wind speed measurements, to reduce thrust at high wind speeds by implementing a blade pitch actuation system, and to design a robust mounting structure to anchor the turbine in a sand bed. To address the safe operation and turbine control, the team opted to use a wind speed sensing device for better state recognition capabilities. To reduce thrust, the team decided to implement an active blade pitching system to control the turbine at high wind speeds and eliminate reliance on a disc brake, except for stopping the turbine during emergencies. With the offshore focus, the team explored and tested numerous pile configurations and sand mat designs to ensure stability during testing.

2.0 Rotor Design

The rotor blade designs were extensively modeled using QBlade and team-designed modeling tools to optimize the design for maximum power production from 5 - 11 m/s. Fabrication of all rotor components was completed in-house. Testing occurred in JMU's wind tunnel and allowed the team to calibrate power production prior to the competition.

2.1 Rotor and Blade Design

A three-bladed horizontal-axis rotor configuration was selected to maximize power production potential of the prototype, due to a high power coefficient (C_p) relative to other configurations. Three blades were chosen for stability and desired torque and rotational speed characteristics over 4 or 5 blade designs. Several candidate rotor blades were designed using QBlade [1], based on airfoils with high glide (C_l/C_d) ratios at low Reynolds number flows (approx. Re = 50,000). Candidate airfoil profiles considered included Wortmann FX60-126 and Wortmann FX63-137 root profiles, and SG6040, SG6042, SG6043, and SG6050 tip profiles. Blade twist was used to achieve the optimal angle of attack to maximize airfoil lift relative to the apparent wind vectors along the length of the blade.

To evaluate and select a rotor blade design, the team compared QBlade simulations of different blade designs and tip speed ratio (TSR) optimizations. A team generated MATLAB script was developed to predict the expected generator voltage and power outputs at different steady state rotational speeds and generator loads when driven by candidate rotor configurations. The power curve performance of each blade was calculated and compared using score weights from Table A-5 in the R&R [2], shown in Table 1. Blades with higher performance scores became the focus of selection. Rotational speeds and

voltage outputs were also considered, to ensure safe operation of the rotor, blades, and electronics with a primary constraint of not exceeding the maximum 60 V input of the selected buck-boost converter.

The selected rotor blade design consists of a Wortmann FX60-126 root airfoil, with a 12.6% chord thickness for structural support, and a SG6042 tip profile, which provides a large lift-to-drag ratio demonstrated in Figure 2 and the associated table. The FX60-126, SG6042 design iterations had higher weighted scores than their counterparts while minimizing highlighted voltage output values. 190-turn and 180-turn generator iterations were not considered due to questionable voltage output modeling results.

Table 1: Modeling results including power output, weighted score, and voltage output predictions at wind speeds from 5 - 11 m/s.

Blade Design	Blade Parameters	Windspeed (m/s)							Total Weighted Score
200 Turn Generator		5	6	7	8	9	10	11	
FX63-137 Root, SG6042 Tip	Power Output	4.64	7.58	12.17	18.10	25.19	33.31	42.28	
	Weighted Score	3.25	6.06	9.73	12.67	10.08	9.99	4.23	56.01
	Voltage Output	49.20	53.00	53.30	55.00	55.00	55.00	55.00	
SG 6050 Root and Tip	Power Output	4.48	7.61	11.89	17.44	24.26	32.00	40.62	
	Weighted Score	3.14	6.09	9.51	12.21	9.71	9.60	4.06	54.32
	Voltage Output	33.80	41.30	50.40	54.00	55.00	55.00	55.00	
FX60-126 Root, SG6042 Tip	Power Output	4.94	8.06	12.94	17.04	23.38	31.36	41.01	
	Weighted Score	3.46	6.45	10.35	11.93	9.35	9.41	4.10	55.04
	Voltage Output	25.70	31.30	35.70	41.20	48.00	54.70	55.00	
FX60-126 Root, SG6043 Tip	Power Output	4.07	7.07	11.45	17.31	24.75	33.76	43.99	
	Weighted Score	2.85	5.65	9.16	12.11	9.90	10.13	4.40	54.20
	Voltage Output	29.20	34.30	39.60	46.90	53.30	55.00	55.00	
190 Turn Generator									
FX60-126 Root, SG6042 Tip	Power Output	4.93	8.03	12.88	18.05	24.58	31.05	40.61	
	Weighted Score	3.45	6.43	10.30	12.63	9.83	9.31	4.06	56.02
	Voltage Output	34.80	43.10	50.00	55.00	53.60	48.50	52.00	
FX60-126 Root, SG6043 Tip	Power Output	4.10	7.11	11.49	17.34	24.73	33.78	44.19	
	Weighted Score	2.87	5.69	9.19	12.14	9.89	10.13	4.42	54.33
	Voltage Output	21.70	29.80	37.50	46.10	51.30	53.20	55.00	
180 Turn Generator									
FX60-126 Root, SG6042 Tip	Power Output	4.91	8.01	12.84	19.19	25.39	31.44	40.23	
	Weighted Score	3.44	6.41	10.28	13.44	10.16	9.43	4.02	57.16
	Voltage Output	32.80	40.70	47.10	53.10	54.70	52.60	54.10	
FX60-126 Root, SG6043 Tip	Power Output	4.07	7.07	11.42	17.23	24.56	33.55	44.08	
	Weighted Score	2.85	5.65	9.13	12.06	9.82	10.07	4.41	53.99
	Voltage Output	20.40	28.10	35.30	43.40	48.20	52.70	55.00	

A similar design, using a SG6043 tip was selected by the 2021 JMU team. At high wind speeds, the observed torque and rotational speed was higher than predicted by QBlade models due to blade roughness and airflow quality. This year's design accounts for these effects to ensure that the rotor does not operate at a speed exceeding generator or power electronics design limits. The rotor was optimized for a TSR of approximately 3.0. Although a larger C_p may be achieved with a higher TSR, the 3.0 design provided the torque necessary to drive the selected loaded generator while limiting operating rotational speeds to approximately 1,750 RPM, thus reducing centripetal forces on the rotor and drive train. Figure 3 shows the simulated C_P-λ performance for the chosen blade design at 0° pitch. Figure 4 shows simulated steady state power production for the selected blade design. At 11 m/s wind speeds, this rotor design is predicted to produce approximately 51 W.

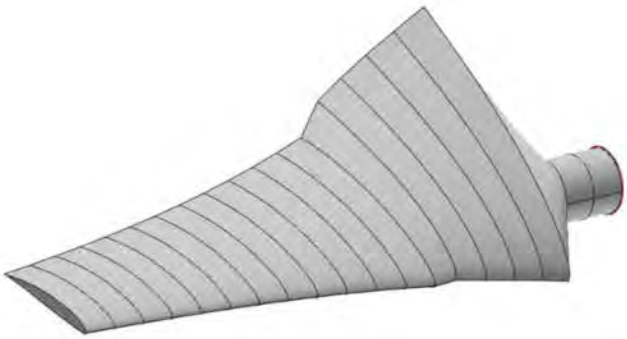

Pos (m)	Chord (m)	Twist (deg)	Foil
0	0.025	0	Circular Foil
0.01	0.025	0	Circular Foil
0.02	0.025	0	Circular Foil
0.03	0.1	36.77	Wortmann FX60-126
0.04	0.096	32.07	Wortmann FX60-126
0.05	0.092	28.19	Wortmann FX60-126
0.06	0.087	24.97	Wortmann FX60-126
0.07	0.081	22.26	Wortmann FX60-126
0.08	0.075	16.96	SG6042
0.09	0.072	15	SG6042
0.1	0.068	13.3	SG6042
0.11	0.065	11.82	SG6042
0.12	0.062	10.53	SG6042
0.13	0.059	9.38	SG6042
0.14	0.056	8.36	SG6042
0.15	0.054	7.45	SG6042
0.16	0.052	6.62	SG6042
0.17	0.049	5.88	SG6042
0.18	0.047	5.21	SG6042
0.19	0.046	4.59	SG6042
0.2	0.044	4.03	SG6042

Figure 2: CAD image of final blade design and detailed design breakdown table - Wortmann FX60-126 Root, SG6042 tip.

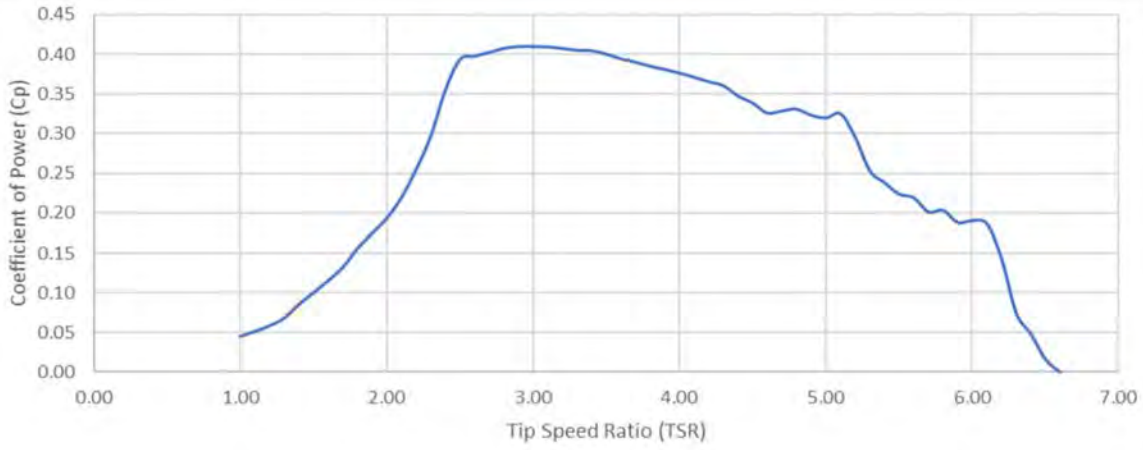

Figure 3: CP vs. TSR for chosen blades demonstrating a Cp of ~0.4 at a TSR of 3.

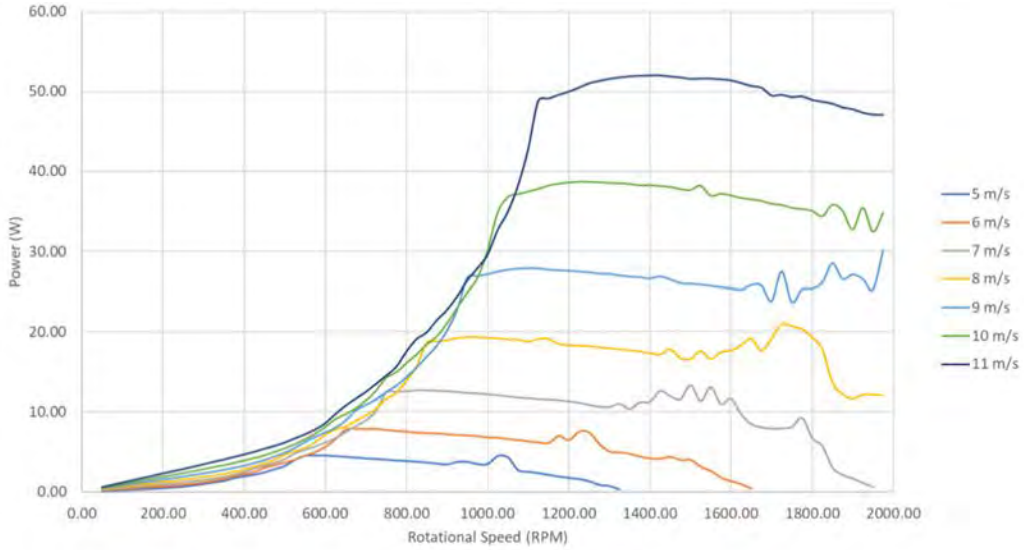

Figure 4: Steady state model of power production for selected blade design.

Blades were 3D printed from Onyx filament [3], a strong and flexible carbon fiber reinforced nylon material, which has been extensively modeled, tested, and demonstrated to withstand required loads. The maximum thrust force experienced by the turbine blades was projected by QBlade to be 10 N at 11 m/s

wind speeds. Deflection testing was performed by drilling holes in the blades, affixing them horizontally, and suspending progressively heavier weights to simulate the thrust force. The point of failure was defined as “deflection that would cause the blades to hit the nacelle” and occurred at 88 N shown in Figure 5, providing a safety factor of 8.8.

Figure 5: Point of failure at 20 lbf (88N) during blade deflection testing.

A maximum centripetal force of 162 N was estimated, assuming a maximum rotational speed of 1800 RPM and measured 28.5 g blades. The 4-40 alloy steel screws affixing the blades have a tensile strength of 170,000 psi, ensuring that the design will withstand the maximum estimated shear forces of 47 psi. To test the integrity of the shoulder bolts holding the blades in place, the rotor was spun at 2500 RPM for 5 minutes at a time. This testing and analysis confirmed that the blades and rotor can withstand the peak thrust and centripetal forces experienced during operation.

2.2 Blade Pitch

To improve turbine control, reduce thrust forces on the tower, and limit overturning forces at the mounting structure, an active pitch system was designed to regulate the rotational speed of the rotor in wind conditions above 11 m/s. A custom designed blade pitching hub, shown in Figure 6, was fabricated to induce blade pitch with a linear actuator.

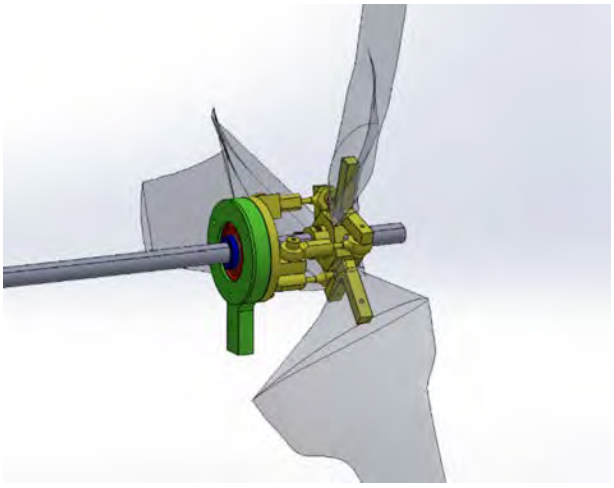

Figure 6: Color coded CAD model of the turbine pitching system. Yellow components rotate with the driveshaft; all other colored pieces do not.

Blades are mounted onto l-shaped aluminum lever arms and fixed using 4-40 thread steel screws. The lever arms are fixed to a hexagonal 6061 aluminum hub with shoulder bolts which allow the lever arms to rotate. Ball joint rods connect the lever arms to a linear-rotary ball bearing based push plate. A non-rotating push-plate is mounted around a rotary ball bearing highlighted in red in Figure 6, which in turn was press-fit onto a linear-rotary bearing colored blue. This configuration allows a non-rotating actuator to vary the blade angle of attack by changing the distance between the fixed hub and push-plate. QBlade was used to simulate the impact of blade pitching on reducing thrust forces at high wind speeds. Figure 7 shows the expected blade pitch angle required to maintain a constant power output for wind speeds greater than 11 m/s. Similarly, this figure shows the anticipated rotor thrust as a function of wind speed when the blades are pitched at these angles. Rotor thrust reaches a maximum of 10 N at 11 m/s and then continues to decrease as the blades are pitched to maintain rotational speed and power output at higher wind speeds.

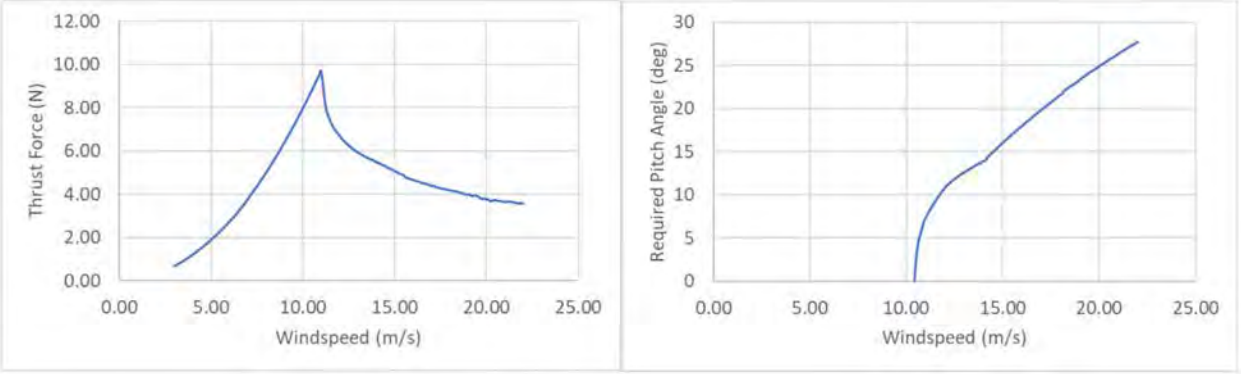

Figure 7: Estimated thrust force experienced by the turbine compared to the angle of blade pitch and pitch angle required at each wind speed

2.3 Rotor Fabrication

The pitching mechanism was fabricated in JMU's machine shop. The circular pitching components and hub were mainly constructed using a lathe and CNC machine. Holes were tapped mainly for 4-40 thread screws, with the exception of the set screw affixing the hub to the driveshaft. 6061 Aluminum was the chosen material because of its lightweight, non-magnetic, and mechanical properties.

3.0 Generator Design

During the conceptual phase of design, the team elected to design and fabricate a three-phase, axial flux permanent magnet generator (AFPMG) because it allowed for optimization of power production when matched with the selected blade design [4]. Although alternatives, including off the shelf motors were considered, an AFPM generator was chosen due to ease of fabrication and customization. The configuration allowed the team to modify the generator voltage output range and efficiency by changing the coil winding density and magnetic air gap [5]. Such flexibility in design allowed the team to match the required torque to power output characteristics of the generator to the chosen rotor blade and electronics design. The generator was the first component manufactured by the team because it represents the critical interaction point between the mechanical and electrical subsystems. All subsequent electronics tests with the system utilized this generator. The size of the generator also influenced all other component dimensions included in the nacelle.

3.1 Generator and Rotor Pairing

A mathematical model, implemented in MATLAB code, was developed to estimate the power produced by a generator and rotor blade design combination at competition wind speeds [6]. The model compared rotor torque and rotational speed characteristics at each wind speed, generated from QBlade models, to the torque required to drive a generator under different resistive loads. In this model, generator design parameters, such as coil winding density and magnetic air gap spacing, were varied to study the impact on power production. The team developed multiple potential generator designs using simulated

data from the preliminary rotor design. To identify the optimal generator configuration, an anticipated power-curve task score, computed using the scoring factors provided in the Rules and Requirements document, was estimated for each candidate generator and rotor pairing configuration. For all simulations, the rectified generator output was limited to 55 V, so as not to exceed the maximum 60 V input of the selected power conditioning electronics. Based on these simulations, the rotor design described above was best paired with a stator consisting of 9-coils, each with 200 turns of 26-gauge magnet wire, wired in a three-phase (3 coils per phase) Wye configuration. This differed from prior JMU design by reducing the number of wire turns per coil to reduce generator voltage and increasing the wire gauge to reduce resistance loss and increase generator efficiency.

3.2 Generator Fabrication

The two generator rotors consist of annular-shaped 416 stainless steel plates with twelve 1 in. x 0.25 in. x 0.25 in. N52 neodymium magnets, arranged in alternating polarities, affixed to one side. Magnetic 416 stainless steel was selected for the plate as it provides low magnetic resistance to close the magnetic circuit and strengthen the magnetic flux through the stator air gap. The team utilized JMU's Machine Shop to fabricate an aluminum hub that affixes each plate to the drive shaft with a set screw and serves as a guide for magnet positioning. The generator stator consists of nine magnetic wire coils, with three sets of three coils soldered together in series to form a phase. The phases were connected in a Wye configuration to produce three-phase alternating current. The hand-wound 26-gauge, 200 turn magnet wire coils were inserted into a laser-cut mold and filled with epoxy resin to solidify the stator's shape. The stator is positioned between the generator rotors using a 3D printed ABS plastic mount. An aluminum spacer was placed between the two magnetic rotors to obtain a fixed magnetic air gap of 1.4 cm.

A focus of this year's effort was to validate the team-designed MATLAB mathematical model by testing the generator on a testing stand that incorporates an AC motor coupled with a torque sensor, shown in Figure 8. These tests allowed the team to verify how generator design variables including magnetic air gap, coil winding density, and flux density impact the loaded generator's drive torque requirements. Figure 9 compares the MATLAB model predictions for torque as a function of rotational speed at different constant operating voltages with experimental measurements of the team fabricated generator design.

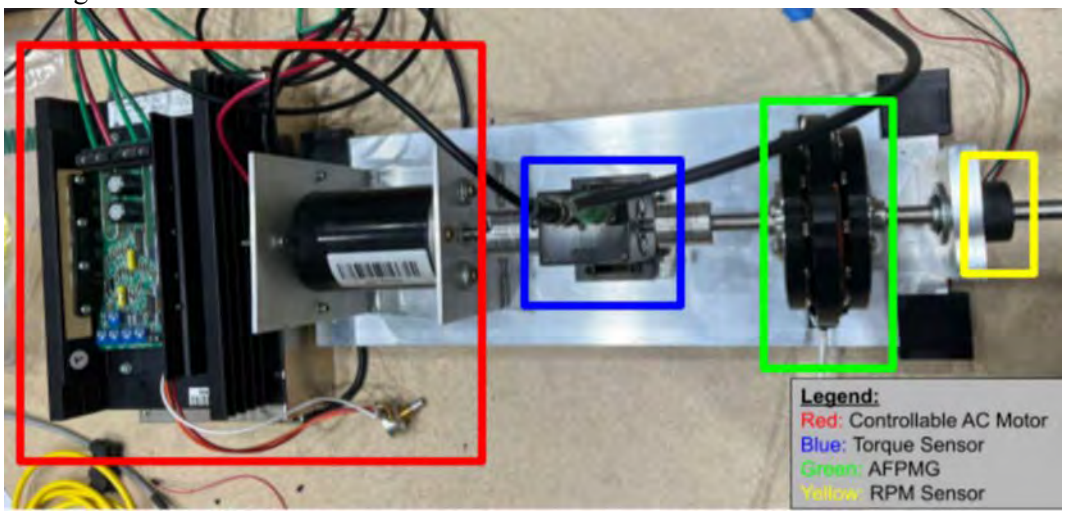

Figure 8: Controllable DC motor powered dynamometer generator test stand.

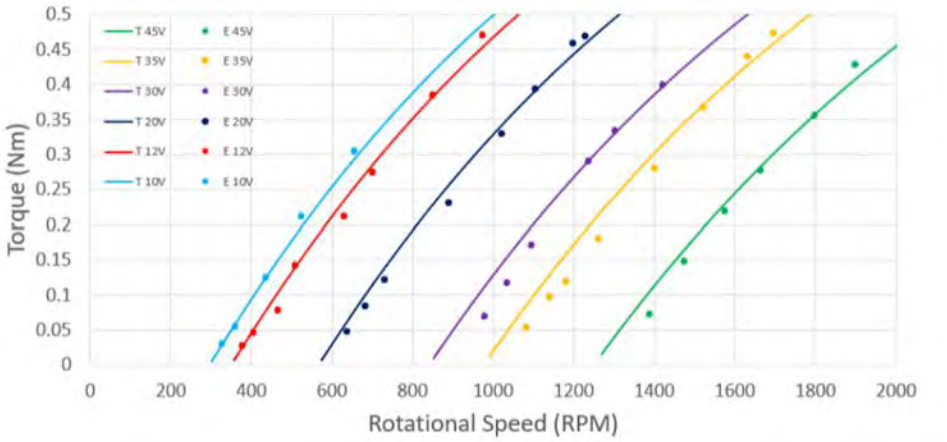

Figure 9: Theoretical (T, solid) and measured (E, points) plot of torque required to drive the AFPMG at different load resistances and voltages as a function of rotational speed.

4.0 Structural and Foundational Design

A new aspect of the competition this year is the inclusion of the fixed-bottom offshore foundation for the turbine prototype. To account for this addition, the team separated nacelle substructure design into two sections: structural design and foundational design, as illustrated in Figure 10. Structural design refers to all non-rotor and non-electronic components that are oriented in the wind tunnel. Foundational design refers to all components located outside of the wind tunnel including the competition-provided transition stub and the team designed fixed-bottom foundation.

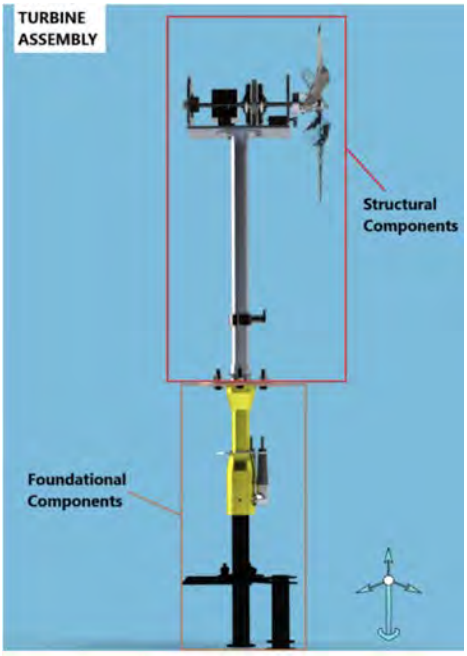

Figure 10: Structural and foundational component callouts of complete turbine assembly.

4.1 Structural Design

The structural components of the turbine include the nacelle, the manually adjustable yaw, the tower, the wind sensor mount, and the baseplate as seen in Figure 11. All structural components, excluding the wind sensor mount, were fabricated from 6061 aluminum.

The nacelle consists of a front, a rear, and a bottom plate that provides structure for mounting the driveshaft, generator, brake system, optical encoder, linear actuators, and Schottky Diode rectifier, as shown in Figure 11. Prior to fabrication and assembly, the nacelle was modeled in SolidWorks to ensure

proper spacing, wire routing, and size. Components are fastened to the nacelle plates using 4-40 thread size, 1/2 in. long button head screws. A D-profile rotary shaft was selected for the drivetrain to reduce the slipping of rotary components. Two sealed ball bearings are press-fit into the front and rear nacelle plates. The turbine's braking system is a cable driven brake caliper, actuated with an Actuonix PQ12 linear servo motor, with an aluminum brake rotor mounted to the driveshaft.

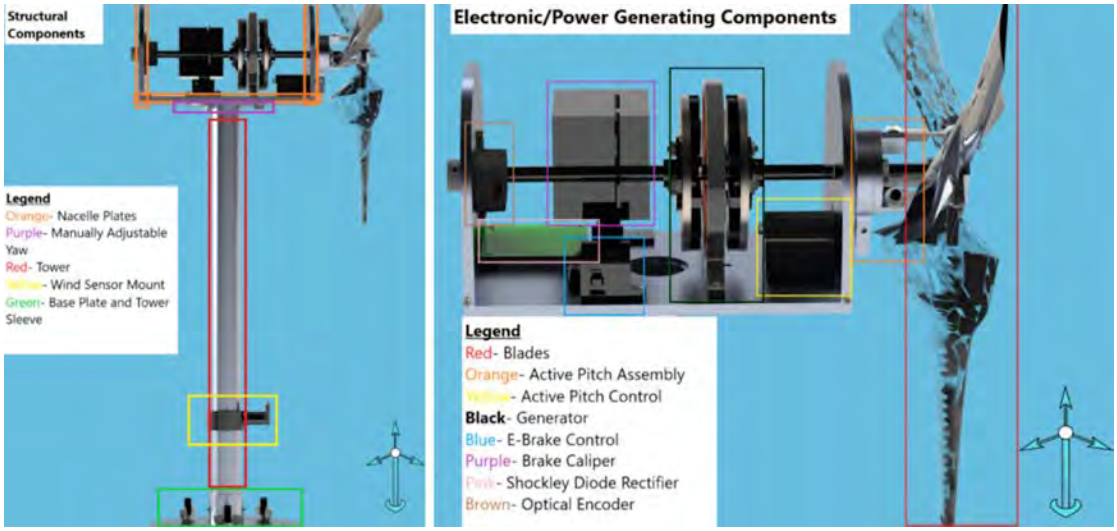

Figure 11: Structural, electronic, and power generating component diagram.

The nacelle rests and pivots upon a flange that is welded to the top of a 54 cm tall tower, which positions the rotor hub 60 cm above the bottom of the wind tunnel. Upon placement within the wind tunnel, the rotor can be oriented in the upwind direction and locked into place. A secondary plate below the flange and the bottom plate of the nacelle exert a compression force on the flange when fastened together by three screws. When the yaw locking screws were tightened to a torque of 1.1 N-m (10 in-lbf), test results, shown in Figure 12, indicated that the nacelle orientation did not change until a moment of 75 in-lbf was applied. The maximum moment expected to be applied to the nacelle is 19.5 in-lbs, yielding a safety factor above 3.5.

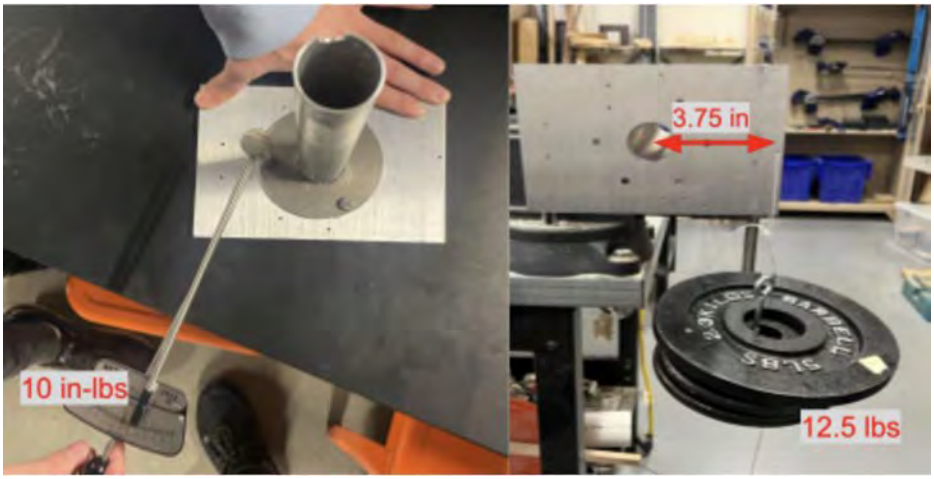

Figure 12: Nacelle lock with safety factor above 3.5.

The turbine tower slides into a metal sleeve that has been welded onto the baseplate. It is then locked into the sleeve via two set screws. There is a hole in the base of the tower and sleeve that allow for the electronic components in the nacelle to be grounded to the baseplate.

The wind sensor mount is located 9 cm from the base of the tower. QBlade wind flow simulations predicted minimal flow velocity reduction at 15 cm below the rotor blades. Similarly, the boundary layer

created from the bottom of the wind tunnel was determined to have an insignificant effect on the wind speeds above 2 cm. Thus, the wind speed sensor mounting location was selected to fall within this height range.

4.2 Foundation Design

To address the new foundation challenge for this year, the team performed a literature review to understand the types of offshore foundations, geotechnical principles, and design parameters. The team opted to focus on a pile-supported structure, eliminating suction caisson, gravity base, floating, monopile, and jacket foundation types from consideration based on competition requirements and the literary review [7]. Current data and equations used to mathematically model offshore foundation design is primarily based on empirical data gathered from tests and large-scale case studies. These modeling techniques were not applicable to a foundation of this project's scale, so the team conducted numerous tests to inform their design.

The team's fixed-bottom foundation is shown below in Figure 13. The team recognizes that on a large-scale application, offshore foundations undergo winds from multiple directions and are typically axisymmetric. However, this foundation was designed for single direction wind flow because the team can infer the wind direction prior to foundation installation, and a single flow design allows for a reduction of weight of the foundation. Based on simulations on rotor thrust, the maximum expected moment the foundation will be subjected to is approximately 10 N-m (7.14 ft-lbf). The design contains three main features: the sand mat, flanged piles, and the foundation tower. All of the main features were constructed from 4130 alloy steel because of its ferrous and machinable properties.

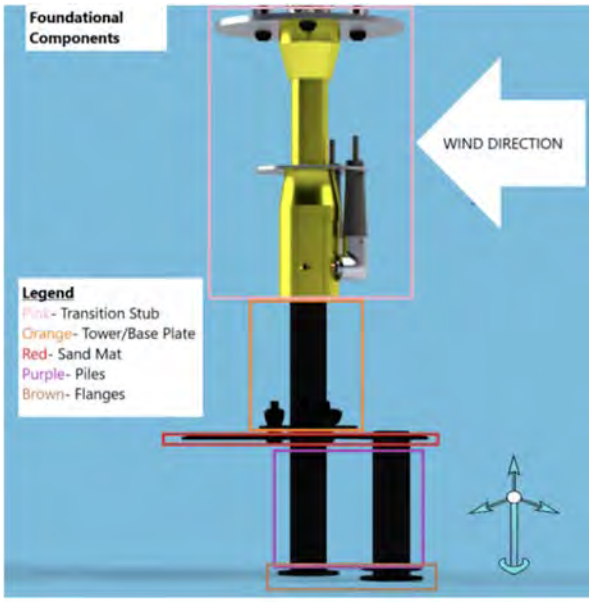

Figure 13: Foundational component diagram.

The sand mat design was fabricated from a 24 cm x 24 cm steel plate. On the upwind half of the plate, sections of plate were removed that were not needed to support the piles to reduce the weight of structure. The downwind half of the plate was left unaltered to generate a greater normal force as the plate drives into the sand.

Three piles were welded to the sand mat; one collinear with the turbine tower and two in the upwind corners of the sandmat. This configuration of piles was determined by using the pile configuration testing fixture seen in Figure 14.

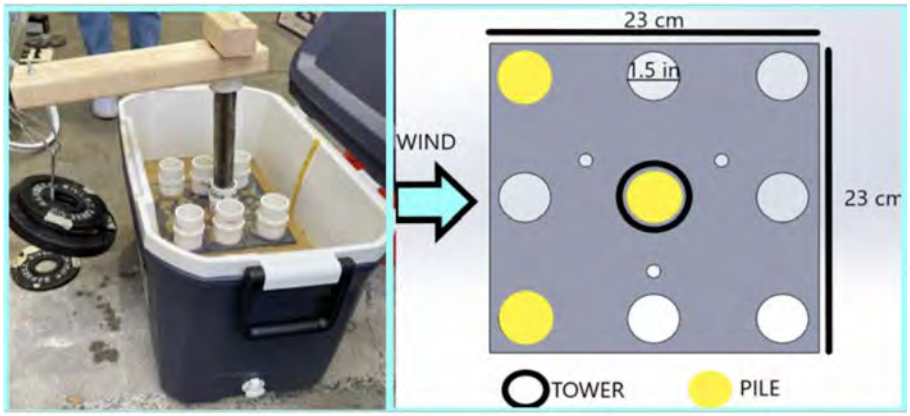

Figure 14: Pile arrangement testing fixture and chosen pile arrangement.

The piles used for testing were 5.75 in. long, 1.5 in. diameter tubing with .058 in. thick walls. The length was chosen because longer piles generate greater lateral loads and the maximum depth of insertion is 6 in. A 1.5 in. diameter pile was selected for consistency with the tower diameter. A thin wall was chosen to decrease the weight of the piles and increase the surface area for generating skin friction. A variety of pile arrangements were tested to their failure point using a torque arm. The chosen three-pile configuration contained the least number of piles that resulted in a safety factor of at least 1.5. The maximum overturning moment the foundation could withstand was 12.5 ft-lbf. Three full scale foundations were then 3D printed with this pile arrangement and tested for uplift force resistance as seen in Figure 15; one with unaltered piles, one with a meshing at the base of the piles, and one with flanges at the base of the piles.

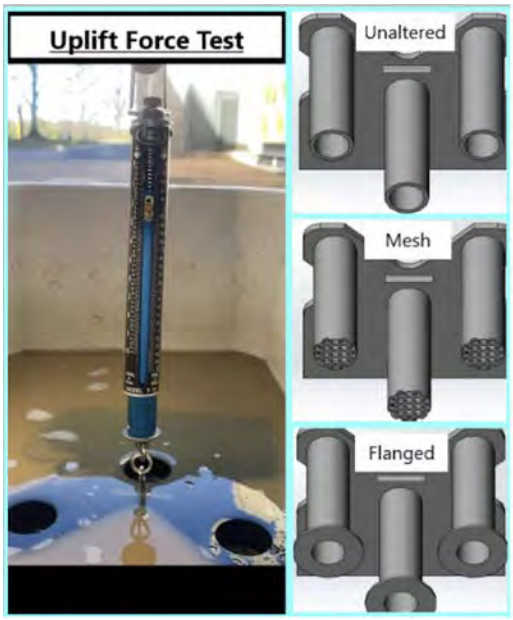

Figure 15: Uplift force test and three pile types.

The flanged pile configuration outperformed the unaltered pile configuration by a factor of 2. From the results of this test, the team decided to weld a flange to the base of each of the piles. The final foundation design was tested to withstand an overturning moment of 32.5 N-m (24 ft- lbf). The addition of the piles had a tradeoff of increasing the weight to increase the safety factor, however the piles only increased the weight of the foundation by 6.7%, but increased the safety factor by about 100%.

The pile supported sand mat is connected to the transition stub by a tower that is welded to a baseplate. The baseplate is secured to the sandmat by three nuts and bolts. There is an opening at the base of the tower so that wires can be routed from the controls to the nacelle. The entire foundation is

assembled and inserted via vibrations generated from a 20 V battery powered Dewalt sheet sander. The sander transfers the vibrations to one pile at a time via metal tubing and 3D printed connections as seen in Figure 16. This method has consistently required approximately 2 minutes for insertion and leveling. The removal of the foundation has consistently taken about thirty seconds.

Figure 16: Process for inserting foundation into sand.

Finite element analysis was conducted on the foundational components to identify weak points in the design. From the von Mises stress distribution diagram, as seen in Figure 17, the areas under the most stress include the upwind base of the foundation tower, and the three fasteners that connect the foundation base plate to the sand mat. The maximum stresses on the foundation are estimated to be 11,620,000 N/m^2. The yield strength of 4130 alloy steel is approximately 460,000,000 N/m^2 yielding a safety factor of 40.

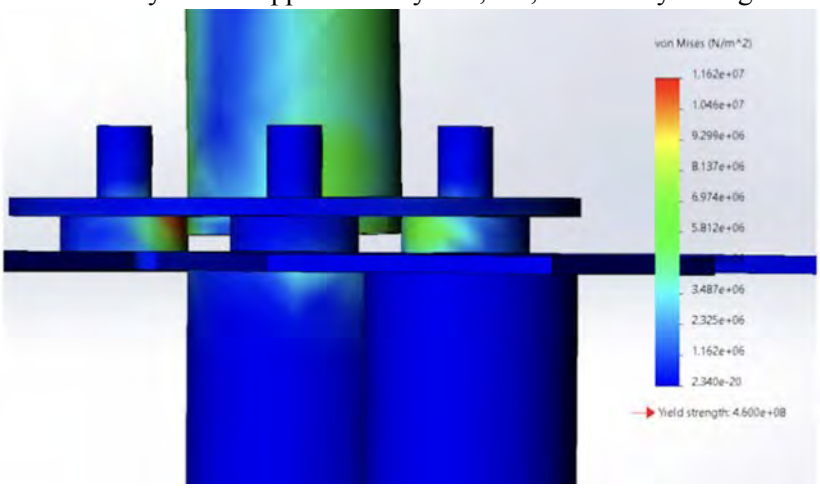

Figure 17: Finite element analysis on foundational components due to oncoming winds.

5.0 Electronics and Controls

The electrical system is designed to safely and efficiently supply maximum power produced by the turbine to the load. Figure 18 presents a simplified schematic of the electronics of the prototype turbine. Three-phase AC power is produced by the AFPMG and rectified to an unregulated DC output with a three-phase Schottky rectifier. The unregulated DC power is then measured by a current and voltage (IV) sensor before being regulated to 12 VDC by a wide range input buck-boost converter. The electronic load is a controlled current sink and power resistor. The power switch and load side motherboard are continuously powered by a 120 VAC to 12 VDC converter that is plugged into a wall outlet. The power switch allows this 12 V supply to be directed to the turbine through the PCC as required for restart control actions, such as releasing the brake, repositioning the pitch actuator after emergency stop actions, and monitoring sensor outputs when the turbine is not producing sufficient power.

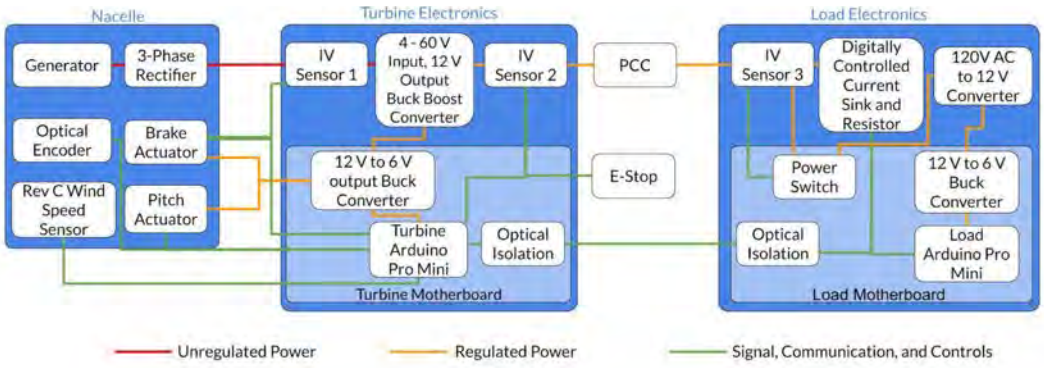

Figure 18: Single line diagram of electrical components and controls.

5.1 Rectification

The three-phase AC output of the AFPM generator required rectification to DC. A MOSFET based ideal diode rectifier specified by the 2020 team and a Schottky diode rectifier were considered for this function. Although less efficient, a Schottky diode rectifier was selected due to ease of manufacturing, reliability, and component availability. Six 60 V, 5 A Schottky diodes, having a forward voltage of 0.52 V, were arranged on a custom designed circuit board in a full wave rectification configuration. At a wind speed of 11 m/s, the generator is expected to produce a current of approximately 0.8 A, resulting in 0.83 W of dissipation by the rectifier.

5.2 Power Regulation and Energy Storage

Unregulated output from the generator is passed from the rectifier to a wide range buck boost converter and is regulated to a constant 12 V. The 12 V output is then distributed to sensors, microcontrollers, actuators, and the load. An off-the-shelf LT8390 buck converter, with an input range of 4-60 V and a constant 12 V output with 4 A output capacity, allows the system to operate over a wide range of rotational speeds without exceeding the 48 V limit at the point of common coupling (PCC). Two additional buck converters are used on each motherboard to step the 12 V input down into 6 V to power the Arduino microcontrollers and each servo motor for the braking and pitching systems. The Arduino then powers all sensors from its onboard regulator supplying 5 V to the IV, RPM, and wind speed sensors. Energy storage on the turbine side electrical system consists of 42 capacitors and 4 inductors on the buck-boost converter, generator and load IV sensors, and motherboard. The inductors range from 1.5 µH to 22 µH and capacitors range from 10 pF to 120 µF. The total energy storage capacity on the turbine side is 0.3 J, well below competition requirements of < 10 J of combined energy storage.

5.3 Sensors

Three custom current and voltage sensors, designed by the 2021 team, monitor crucial points of the system's power path. The first sensor is placed to measure current and voltage immediately after the rectifier, the next following the buck boost converter, and the third on the load side after the PCC. The boards are designed with voltage divider configurations and shunt current amplifiers to condition measurements for the Arduino's analog input.

U.S. Digital E5 optical encoder with a 100 count per revolution resolution is used to measure the rotational speed of the drive shaft. The Arduino can measure the square output waves and convert them into an estimated rotational speed. Due to the timing resolution of the Arduino Pro Mini, the team can read measurements ranging from 10 RPM to over 10,000 RPM, well over prototype operating conditions.

New for the 2022 team, a Modern Device Rev C. Wind Sensor [8] will be introduced to have a direct measurement of incoming wind speeds. The sensor operates based on a hot-wire anemometer principle, measuring the current required to maintain the temperature of a resistive element. Sensor voltage output is sent to the microcontroller, where calibration data is already in place to accurately identify the incoming

wind speed. The sensor will assist in state identification for control and positioning of the active pitching mechanism.

5.4 Load Configuration

The load system, represented schematically in Figure 19, is an analog controlled current sink with a 2.7 Ω resistor. The load system consists of an error amplifier with two inputs; a digital-to-analog signal commanded by the Arduino and the output of an instrumentation amplifier used to measure the potential difference across a 5 mΩ shunt resistor. The output of the error amplifier controls the gate voltage of an N-channel MOSFET to make the difference between the two inputs as close to zero as possible. This makes the current measured through the MOSFET and power resistor match the current command sent from the Arduino. A heat sink is used on the MOSFET to remove the increase in temperature as it is simulating a resistor. The power resistor used as the load is rated for 100 W with high current handling and no current derating. This configuration is the same as the 2021 team as it was proven to ensure power quality and stability to the load.

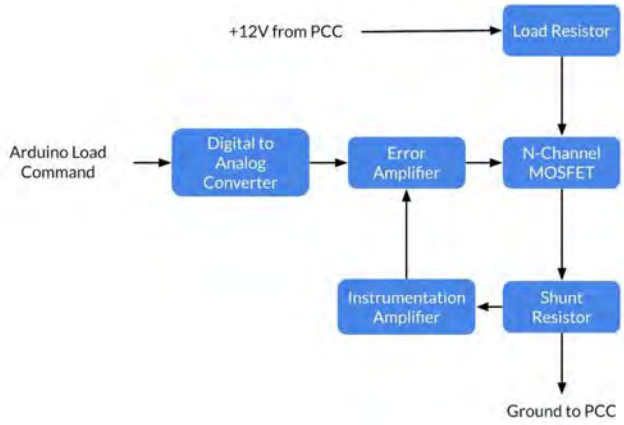

Figure 19: Load schematic for the analog controlled system.

5.5 Controls

Initially the controls subteam was planning to use Python to run calibration and control programs, but with a long history of Arduino knowledge and familiarity, the team decided to use two Arduino Pro Mini microcontrollers. The Pro Minis have 6 analog input pins that allow the team to incorporate the wind speed sensor into the design and enhance state identification capabilities. The Pro Minis are considerably smaller, consume less power, and maintain the required functionality as the previously used Pro and Uno boards in the 2021 turbine prototype. The load side controller is always powered and is the primary system controller. The turbine side controller monitors sensor outputs, sends control signals to the brake and pitch actuators, and tracks emergency conditions. The two controllers exchange information and commands via a 57,600 baud serial connection that is optically isolated with two HCPL 2200 ICs.

The main operating states are briefly described below and schematically shown in Figure 20.

- Start/Restart State (States A, B, or X): Identified by lack of power to the turbine, no communications from the turbine, or serial communications disconnected. If emergency stop conditions are not present, power is provided from load to release the brake and reposition pitch to startup state.
- Cut-in (State C): Wind speeds below 5 m/s, low rotor rotation speed. No load, power with +12 V from turbine. Slight pitch to feather to increase torque experienced at the generator.
- Power Curve (States D, E, and F): Wind speeds between 4.5 m/s - 11 m/s. Pitch to zero, control load to maximize power, and maintain rotational speed.
- Control of Rated Power (State G): Wind speeds 11-22 m/s. Adjust pitch based on measured wind speed to reduce rotational speed and rotor thrust. Adjust load to maintain rated operating speed and maximum power.

- Cut out (State H): Above 22 m/s. Pitch turbine rotor, activate parking brake.
- Emergency Stop (State K): When emergency stop button disconnect is detected, activate the disc brake. Initiate restart once the emergency stop condition is removed.
- Power Disconnect (State L): Monitor turbine output voltage and load input voltage. If there is a significant difference between the two, active brake. Initiate restart state.

For every cycle, the main controller validates if communications from the turbine have been received. If there is no communication the load understands that the turbine is either in the parked position, communications have been disconnected, or the wind speed is insufficient to power the turbine electronics. When these conditions are observed, the primary controller provides power to the turbine, commands the controller to release the brake, and return the active pitching actuator to the starting position.

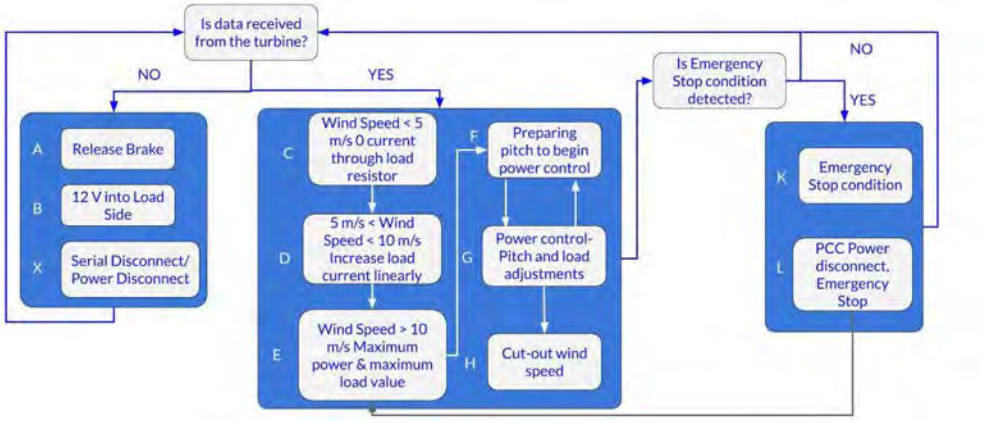

Figure 20: Turbine control states diagram.

When communication is received, the controller determines the operating state based on the wind speed and adjusts the load current, brake, and pitch settings accordingly. During pre cut-in wind speeds, the load acts as an open circuit to allow all generated power to be consumed by the turbine electronics. Once cut-in is reached, the controller gradually increases the current setting in a linear progression as wind speeds increase. Above 6 m/s, the controller enters a maximum power tracking state. Adjustment of the load is achieved by monitoring the wind speed and rotational speed measured. The load current command is adjusted proportionally to the difference between the observed and optimal rotational speed. If the measured speed is higher than anticipated, the load will allow more current to pass and slow the rotor. Similarly, with a slower expected rotational speed, the load will reduce the amount of current that is passed to the load and speed up the rotor to make up the difference.

When wind speeds above 11 m/s are measured by the wind speed sensor. The active pitching system engages and begins to pitch the rotor. The pitch position is determined based on the measured wind speed. Once the pitch is set, the load algorithm acts as a fine tuner to match the expected rotational speed at each wind speed above 11 m/s. The final state the turbine checks is the emergency stopping condition. The manual E-stop is identified by a change in the button state monitored by the primary load side controller. The PCC power disconnect is identified by the voltage difference on both sides of the PCC. If either emergency condition is observed, the brake is engaged fully to stop the rotor by a disc brake.

6.0 New for 2022 Design

JMU has been a regular participant in CWC since 2018. The TWC team's prototype is the product of each subsequent team's experiences and knowledge. As a result of this, the 2022 TWC team's design differs from the 2021 design in most aspects. The rotor is a combination of two airfoils, the Wortmann FX60-126 & SG6042, the previous team also incorporated the Wortmann FX60-126 but with a different tip profile. Never achieved by previous teams, this year's design will pitch the blades at high wind speeds with an active pitching mechanic. The AFPM generator design was opted to be used again like previous

teams but the parameters changed to 9-coil 26-gauge wire with 200 turns to optimally match our rotor selection instead of 28-gauge wire with 225 turns used by the 2021 team.

With a focus on offshore development, the team identified the critical functions and requirements for the structural and foundational components. The 2021 team incorporated a passive yaw system that was replaced by a fixed yaw with a manual locking system. The electronics incorporated in this year's design are identical with the exception of the wind speed sensor for better state identification abilities. As a result of the wind speed sensor and active pitching mechanic, the control algorithm for the prototype is vastly different from previous years. A power tracking algorithm was developed for the 2021 team that determined the state of the turbine. At high wind speeds, the brake was engaged to slow the driveshaft. The 2022 team can identify state conditions through the wind speed sensor and encoder data. At high wind speeds, the active pitch will engage to stall the rotor and control the rated power produced.

7.0 Full Turbine Assembly

Full turbine assembly was achieved by constant communication between the subteams and step wise integration techniques to consistently test the functionality of subsystems. The mechanical drawing and exploded view of each turbine component can be seen in Figure 21. The team was able to successfully complete most competition contests in the JMU home-built wind tunnel with the exception of tests requiring wind speeds above 9.5 m/s and the Control of Rated Power Task. The team documented all calibration and testing data to estimate performance and score according to the R&R scoring rubric.

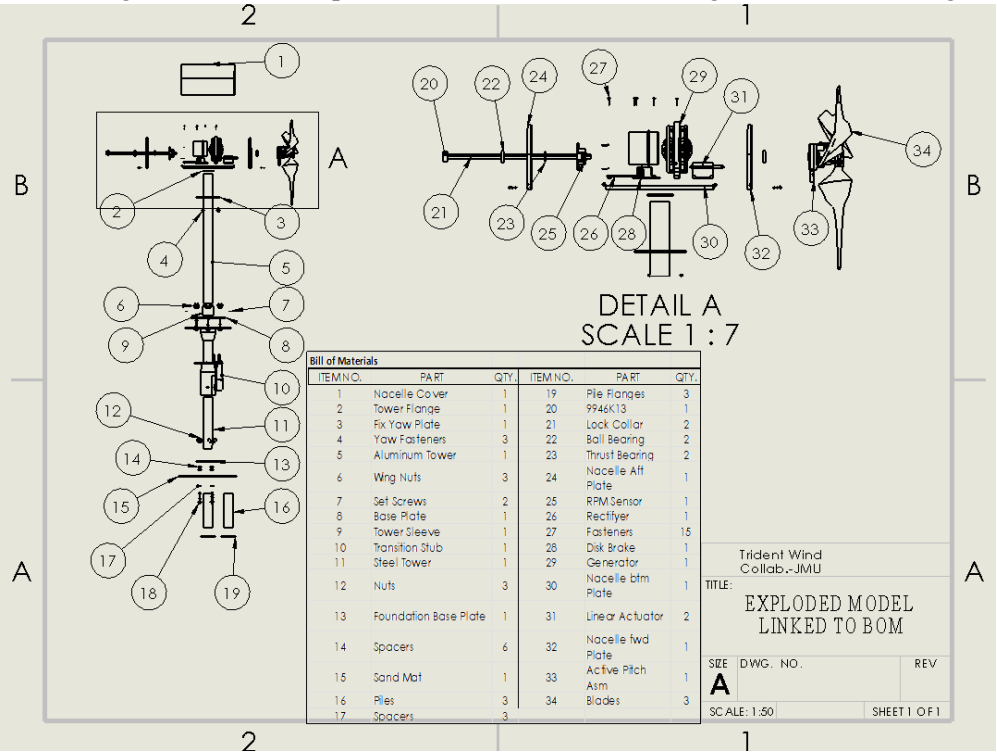

Figure 21: Full turbine exploded view.

7.1 Safety Inspection

The team initiated several safety checks at various stages of integration. Dr. Keith Holland, the team's capstone advisor, conducted initial safety inspections prior to testing in the in-house wind tunnel. The team also enlisted the help of Computer Engineer and Associate Professor Dr. Jason Forsyth and Engineering Lab manager, John Wild, to conduct the Safety and Tech Inspection Sheet provided in Appendix B of the R&R.

7.2 Cut-in Wind Speed

Sporadic power was observed at 4.5 m/s while reliable power was recorded at 4.7 m/s. Therefore, the cut-in speed of the turbine is 4.7 m/s. Considering drivetrain friction, electrical load, and a cut-in speed of 4.7 m/s, QBlade estimates that a torque of 0.08 N*m is required to begin producing power. With the active pitching system, the team can slightly feather the blades to cut-in at lower wind speeds and return to a zero pitch angle after power is observed.

7.3 Power Curve Performance

The turbine was tested in the in-house wind tunnel at a range of wind speeds up to 9 m/s to determine the maximum power curve. At each wind speed from 4.7 - 9 m/s the voltage, current, power output, wind speed, and rotational speed were recorded. Figure 22 presents the measured and projected generator power in blue and the measured and projected power delivered to the load in orange. Note that the measured generator power is similar to that anticipated through modeling while the power delivered to the load is reduced due to electrical and mechanical losses.

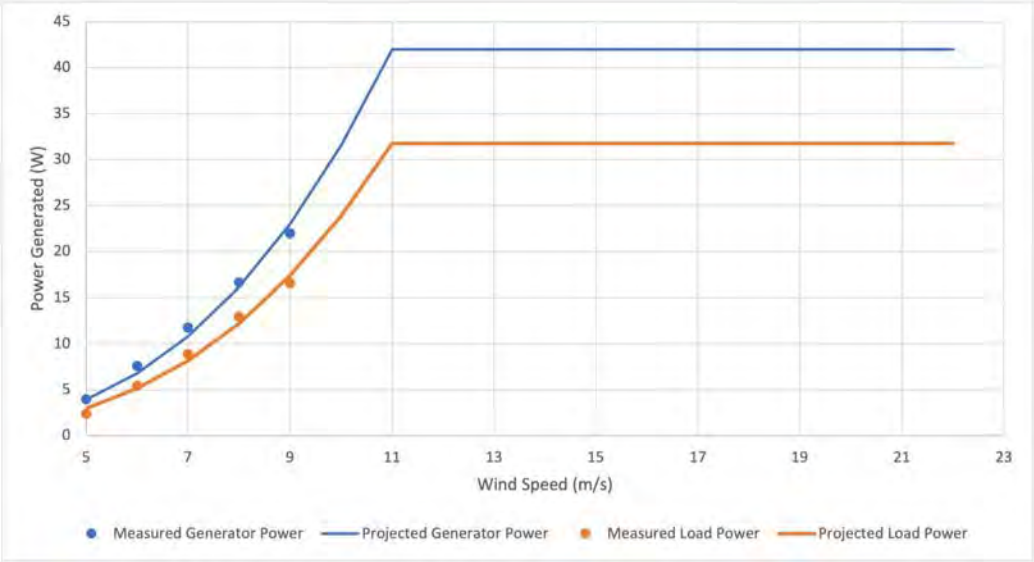

Figure 22: Measured and anticipated power production at competition wind speeds.

The measured results indicate an end-to-end wind power to load power efficiency of 24.5%. Assuming a rotor C_p of 0.38, the generator mechanical-to-electrical power conversion efficiency was estimated to be 85%, consistent with model predictions. This suggests an electrical conversion and transfer efficiency of 76%. These measurements and estimates are reasonable due to the power consumption from the turbine electronics, sensors, actuators, and the anticipated 85% buck-boost converter efficiency [9]. Through calibration testing, the team also identified that the simulated TSR values were close to the observed values, shown in Table 2.

Table 2: Comparison of expected and measured RPM and TSR.

Wind Speed	**5 m/s**	**6 m/s**	**7 m/s**	**8 m/s**	**9 m/s**
Simulated	765.80 RPM TSR = 3.0	1024.81 RPM TSR = 3.0	1199.36 RPM TSR = 3.0	1415.10 RPM TSR = 3.0	1674.38 RPM TSR = 3.0
Measured	824.21 RPM TSR = 3.22	1017.62 RPM TSR = 2.97	1188.43 RPM TSR = 2.97	1408.21 RPM TSR = 2.98	1652.32 RPM TSR = 2.96

7.4 Safety Task

The turbine was run through one of the two safety tests by demonstrating a safe stop during the E-stop shutdown. The turbine was able to successfully come to a complete stop when the E-stop switch was initiated. Following each shutdown condition, the turbine was able to successfully restart and return to a power producing state. Prior to competition, the team will test the second shutdown condition by disconnecting the load and turbine electronics.

8.0 Prototype Testing Commissioning Checklist

A checklist to verify each step of assembling the turbine during the competition is provided in Table 3. This checklist includes a team member responsible for performing each verification step and a person responsible for verifying that each step is performed correctly.

Table 3: Commissioning checklist for turbine assembly.

Verification Step	**Initiating Team Member Initials**	**Verification Team Member Initials**
Gather foundation and insertion materials: Pile-supported sand mat, tower and baseplate, spacers, sander with fully charged 20 V battery, and vibration transfer tubes	**CS**	**MP**
Place electrical cable through the foundation tunnel and base plate.	**CS**	**MP**
Fasten the base plate to the sand mat.	**CS**	**MP**
Place vibration transfer tubes onto upwind piles.	**CS**	**MP**
Place the assembled foundation into the tank with piles facing in the upwind direction.	**CS**	**MP**
Apply vibration from sander to one pile at a time until the sand mat is flush with sand bed.	**CS**	**MP**
Check the top of the tower for levelness and make adjustments with sander to make the foundation level.	**CS**	**MP**
Attach a transition stub so that one bolt of the flange assembly is pointing in the downwind direction.	**CS**	**MP**
Slide foundation tank under the center of the wind tunnel.	**CS**	**MP**
Connect wires from the nacelle to the foundation connection point	**CS**	**MP**
Fasten the turbine base plate so that the wind sensor is perpendicular to the incoming wind flow.	**CS**	**MP**
Ensure the nacelle is oriented in the upwind direction, then tighten the fasteners on the manually adjustable lock plate to 10 in-lbs	**CS**	**MP**
Connect and verify Anderson Power Pole Connection from tower to turbine electronics.	**AD**	**GD**

Connect and verify Anderson Power Pole Connection power connection to PCC from the turbine.	**AD**	**GD**
Connect and verify Anderson Power Pole Connection power from PCC to load	**AD**	**GD**
Connect and verify Serial communications cable	**AD**	**GD**
Plug load AC/DC adapter to outlet	**AD**	**GD**
Confirm receipt of Serial communications and startup state of turbine	**AD**	**NP**
Engage E-stop to verify servo operations	**AD**	**NP**
Remove E-stop	**AD**	**NP**
Verify cut-in at 4.7 m/s wind speed	**AD**	**NP**
Verify receipt of wind speed measurements.	**AD**	**NP**
Verify the voltage and current readings through all IV sensors	**AD**	**NP**
Confirm receipt of rotational velocity measurements	**AD**	**NP**
Alert judges to commence testing sequence.	**AD**	**BS**

References

[1] Hermann Föttinger Institute of TU Berlin. (2014). QBlade: an Open Source Software Version (v0.8).

[2] "Rules and Regulations." US Department of Energy. September 2021. https://www.energy.gov/eere/collegiatewindcompetition/articles/collegiate-wind-competition-rules-and-requirements

[3] "800cc Onyx Filament Spool." *Markforged*, 11 Dec. 2021, https://markforged.com/product/onyx-filament/.

[4] Price, G., Batzel, T., Comanescu, M., & Muller, B. (2014). Design and testing of a permanent magnet axial flux wind power generator (Paper 190, ENT 202). International Association of Journals & Conferences.

[5] Kao, J. –Hsiang, Lin, Y.-J., & Huang, Y.-W. (2020a). Apply blade element momentum theory in matching a wind turbine system. International Journal of Smart Grid and Clean Energy, 44–51. https://doi.org/10.12720/sgce.9.1.44-51

[6] Kao, J.-H. (2016). Developing the process in matching a wind turbine system to attain optimal performance. Advances in Mechanical Engineering, 8(11), 168781401667469. https://doi.org/10.1177/1687814016674697

[7] Lavanya, C., & Kumar, N. D. (2020, August 19). *Foundation types for land and offshore Sustainable Wind Energy Turbine Towers*. E3S Web of Conferences. Retrieved March 11, 2022, from https://www.e3s-conferences.org/articles/e3sconf/abs/2020/44/e3sconf_icmed2020_01094/e3sconf_icmed2020_01094.html

[8] "Wind Sensor Rev. C." Modern Device. April 18, 2022. https://moderndevice.com/product/wind-sensor/

[9] "Demo Manual DCA - Analog Devices." April 24, 2022, https://www.analog.com/media/en/technical-documentation/user-guides/DC2457AF.PDF